

Kink-Helium Interactions in Tungsten: Opposing Effects of Assisted Nucleation and Hindered Migration

Matthew Nutter,^{1,2,*} James R. Kermode,² and Albert P. Bartók^{1,2}

¹*Department of Physics, University of Warwick, Coventry CV4 7AL, United Kingdom*

²*Warwick Centre for Predictive Modelling, School of Engineering,
University of Warwick, Coventry CV4 7AL, United Kingdom*

Point defects such as interstitial atoms are known to be attracted to screw dislocations. Understanding these interaction mechanisms is key to predicting the plasticity of real materials. Using a potential derived from *ab initio* calculations of helium in tungsten, we find that the binding of a helium atom to dislocation kinks is significantly more favorable than to a straight dislocation. This preference directly translates to a reduction in the kink pair nucleation energy, provided that the mechanism proceeds through a helium-stabilised kink. It is lowered from 1.64 eV (in the pure metal) to 0.51 eV when helium binds to the right kink. However, binding also has a competing effect whereby the kinks are unable to migrate. This hindering aspect becomes more relevant as the helium concentration increases.

© 2024 British Crown Owned Copyright / AWE

Tungsten is a primary candidate for the plasma-facing armour components of future nuclear fusion reactors, due to its high melting point, resistance to radiation damage, and thermal conductivity [1]. Helium atoms will be present from the fusion process and transmutation reactions. Such interstitial defects are believed to interfere with the movement of screw dislocations with $\frac{1}{2}\langle 111 \rangle$ Burgers vector, b , which typically propagate through the crystal by thermally activated nucleation and migration of kink pairs. Since the plasticity of body-centred cubic metals such as tungsten is largely determined by the movement of these dislocations, it is crucial to have a detailed understanding of how they behave in the presence of impurities to ensure the durability of these components. Predictions indicate that after five years, reactor components may have helium concentrations of up to 20 appm [2], a level that has been demonstrated in experiments to suppress recrystallisation and increase the ultimate tensile stress [3]. However, in such dilute regimes, the influence of helium on dislocation motion is less well understood.

In this letter, we demonstrate how the interaction of helium with dislocation kinks has a significant impact on screw dislocation mobility, by assisting kink pair nucleation and hindering kink migration. This is accomplished by building a Machine Learning Interatomic Potential (MLIP) from *ab initio* data for low concentration helium in tungsten. The large time and length scales that are required to study dislocation mobility are well beyond the limits of density functional theory (DFT), due to its computational cost which typically scales cubically with the number of electrons. Kink pairs break the symmetry along the dislocation line, thus ruling out the possibility of a short simulation cell that is periodic along the dislocation line. Additionally, large cells are required to limit the self-interaction of impu-

rities through periodic boundaries and allow for long-range relaxation of the dislocation core (i.e., the region immediately surrounding dislocation lines, where the crystal structure is most distorted). Recent work with hybrid quantum-mechanical/molecular-mechanical (QM/MM) methods has allowed for a quantum accurate description of impurity-dislocation interactions on a larger length scale [4]. However, these simulations require force integration to obtain energy differences and are restricted in time by the cost of the DFT calculation used in the quantum region and the need for large ‘buffer’ regions to mitigate the effects of artificial surfaces [5]. Training MLIPs provides access to larger time and length scales, whilst aiming to maintain quantum accuracy.

Building the ab initio database — Using the Gaussian Approximation Potential (GAP) framework [6, 7], we build upon a MLIP for screw dislocations in tungsten [8], with the aim of improving the accuracy of dislocation kinks and helium-induced core reconstructions. This requires the training database to include configurations with relevant atomic environments. All configurations in this work were evaluated using the CASTEP planewave DFT code [9]. To build the database efficiently and keep the number of atoms low, we use a quadrupolar periodic array of dislocation dipoles [10]. It was found that the widely used 135 atoms/ b simulation cell could be compressed further into 45 atoms/ b (built following the convention in [11] with $n, m = 9, 5$). The dislocations are separated by approximately 12 Å in the 45 atoms/ b geometry (versus 19 Å for 135 atoms/ b), which if used for direct *ab initio* studies would result in undesirable finite-size effects [12]. However, the minimally strained tungsten atomic environments that separate the dislocation cores in the 135 atoms/ b cell are adequately covered elsewhere in the database. The compressed cells have proven to be invaluable for collecting energy and force data for atomic environments near dislocation cores, for otherwise unobtainable dislocation line and kink sizes (up to 10 b in length). Testing confirmed that MLIPs

* m.nutter@warwick.ac.uk

trained on 45 atom/ b configurations make predictions on unseen 135 atom/ b configurations with reduced errors compared to those without them. Further details surrounding the MLIP fitting and training data can be found in the Supplementary Material [13] (see also references [14, 15] therein).

Helium-induced core reconstructions — In pure bcc metals, the ground state of the screw dislocation lies at the centroid of three [111] atomic columns, often referred to as a Peierls valley. The dislocation core structure in this case is known as the *easy core* and the presence of helium leads to spontaneous reconstruction away from this ground state [4].

When the dislocation line is saturated with one helium atom per b , the resulting reconstruction is known as the *hard core*, where atoms in the three atomic columns surrounding the core lie in the same plane [4]. The hard core is an unstable maximum in the potential energy landscape of the pure metal [11]. If modelled in a $1b$ cell, the helium atoms are constrained to exist in a periodic array. When the translational symmetry along the dislocation line is allowed to break (cell length $> 1b$), we find that this periodic arrangement is not the most stable. We observe that, similar to in bulk [16], it is preferential for helium atoms to form clusters (by 0.13 eV/He in a $2b$ cell), while maintaining the hard core structure (see Supplementary Material [17]). We validated this result with DFT, but did not explore longer line lengths. Nevertheless, this observation emphasises the need for large cells (and therefore cheaper methods, such as MLIPs), even in the saturated regime, due to the intricate arrangements that may form around the core.

Our simulations predict that in the dilute regime, where a single helium atom is situated within a sufficiently long dislocation line, the dislocation core reconstructs towards the *split core* in the vicinity of the helium. This is another maximum in the energy landscape of the pure metal, where the dislocation lies close to a [111] atomic column. Away from the helium atom, the dislocation core structure gradually reverts to the easy type over a distance of approximately $10b$, in agreement with previous QM/MM studies [4].

Dislocation-helium interaction energies — Point defects are drawn to dislocations due to the attraction of their respective stress fields. The corresponding interaction energy can be calculated using

$$E_{\text{int}} = E_{\text{dis}} - E_{\text{dis+He}} - (E_{\text{bulk}} - E_{\text{bulk+He}}), \quad (1)$$

where E_{dis} and E_{bulk} are the energy of a pure tungsten simulation cell with and without a dislocation, respectively. $E_{\text{dis+He}}$ and $E_{\text{bulk+He}}$ are the energy of the same simulation cells, but with a helium atom at the most stable site. We obtain a value of 1.69 eV for the binding of helium to the straight dislocation in the dilute regime. This differs slightly from the published QM/MM result of 1.5 eV [4]. Our *ab initio* calculations yield a value of 1.52 eV (Figure 1) with finite-size effects — both in-plane and along the dislocation line — that reduce the energy.

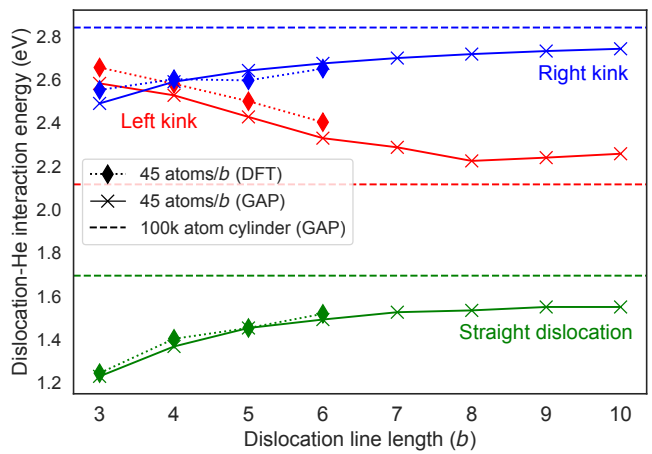


FIG. 1. Convergence of dislocation-He interaction energies. Diamonds and crosses represent DFT and GAP calculations in 45 atoms/ b quadrupolar cells, respectively. Horizontal dashed lines are converged values obtained in large cylindrical cells with GAP. Bulk(+He) references are calculated in 432(+1) atom cells.

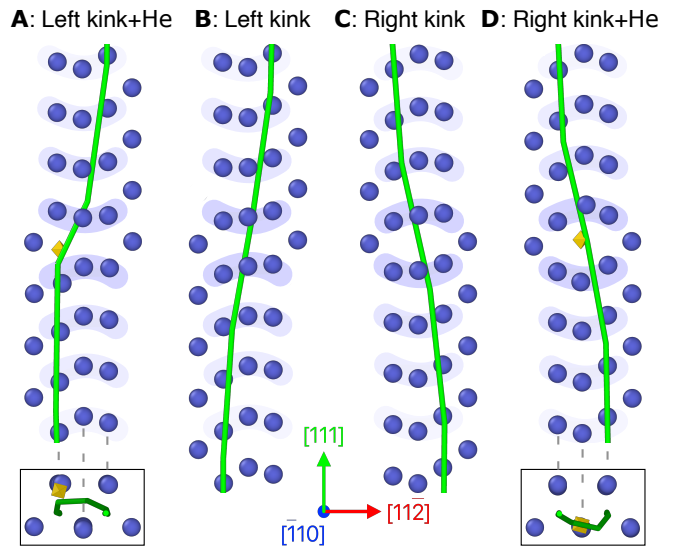


FIG. 2. The left (interstitial) and right (vacancy) kinks, with and without helium, A-D. Only atoms around the dislocation are shown, with highlighting to emphasize the character of the kinks. Dislocation lines (in green) are from Ovito’s dislocation analysis [18]. Insets show the view down the [111] direction.

Therefore, we argue that the difference here, at least in part, is due to differences in DFT codes and/or surface effects from the QM cluster, despite a buffer region, in the QM/MM case.

Periodic arrays of individual dislocation kinks (from the kink pair) can be constructed using appropriately tilted cells [19], allowing for the energy of their interaction with helium to be calculated. We observe significant increases in binding compared to the straight dislocation for both the left and right kink (also known as the in-

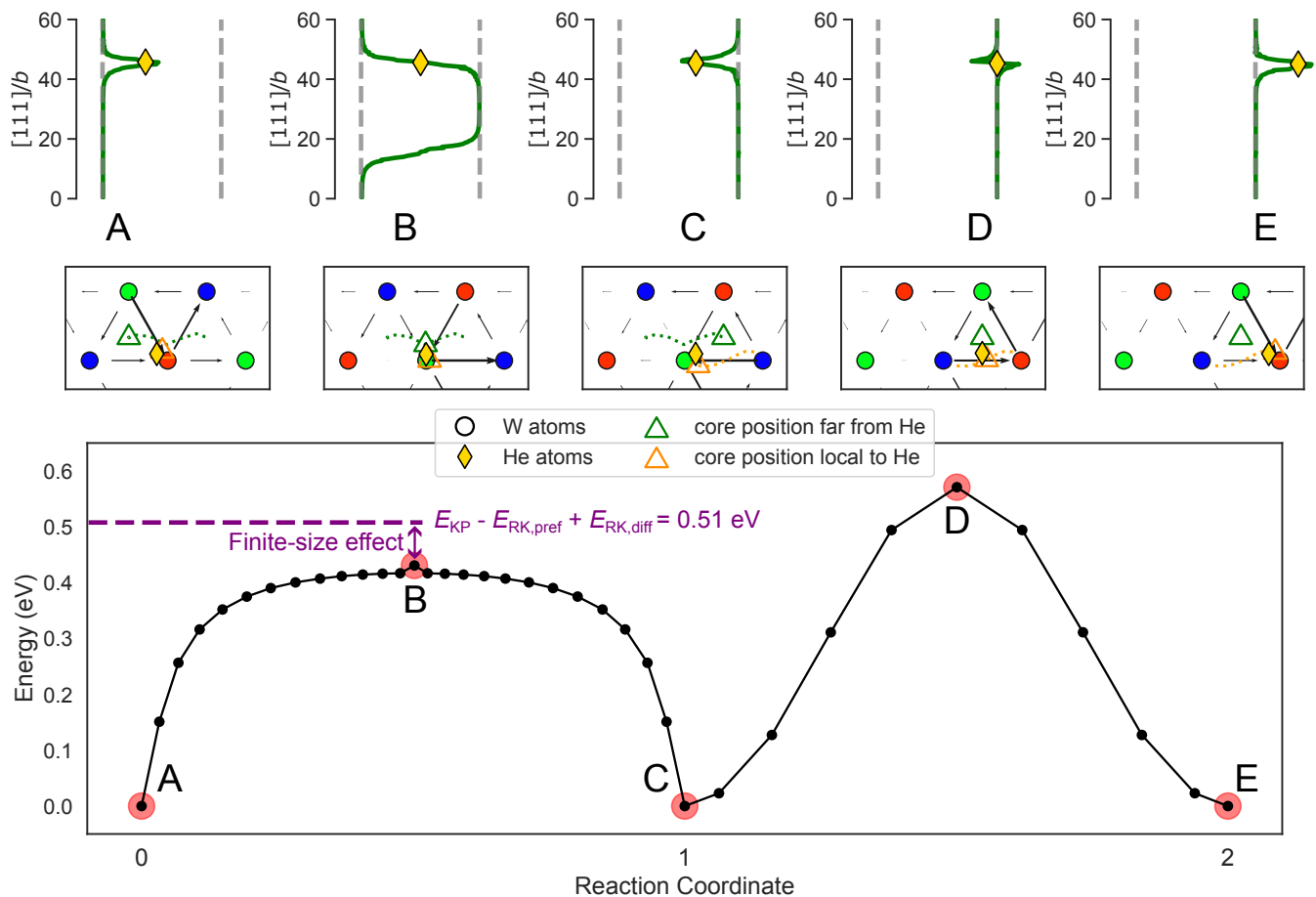


FIG. 3. Two-step NEB pathway for helium-assisted kink pair nucleation. A→C: Kink pair nucleation through helium-stabilised right kink, with left kink migration. C→E: Diffusion of helium to the next [111] atomic column. Dislocation line positions (determined using the cost function method [11]) as they move between Peierls valleys (grey dashed lines), and differential displacement maps (for the layer that is local to helium) are shown for the key images. Green and orange dashed lines on the differential displacement maps represent the path taken by the dislocation far ($30b$) from and local to the helium, respectively. The triangles correspond to the position in the current image. The reaction coordinate is normalised by average dislocation position for A→C and by helium position for C→E.

terstitial and vacancy kink, due to local compression and tension in the centre [20, 21]), with a binding energy of 2.12 eV and 2.84 eV, respectively. Therefore, the preference for kink binding is ~ 0.4 eV and ~ 1.1 eV for the left and right kink, $E_{LK,pref}$ and $E_{RK,pref}$. The large preference allows us to partially validate our result in small cells solely with DFT (Figure 1), since the finite-size errors do not mask the qualitative behaviour. The vacancy character of the right kink may explain its greater affinity for helium compared to the left kink, whose interstitial character results in the helium atom not binding to the central [111] atomic column. This can be better understood by looking at the structural changes of the three [111] atomic columns around the kink (highlighted in Figure 2). We observe the opposite trend for the preferred [111] column when a vacancy binds to the kinks, but for quantitative analysis the GAP needs to be further extended with relevant representative configurations.

In the case of the left kink, we find that the entire dislocation line can move out of the initial (110) plane, such that the [111] column accommodating the helium atom becomes the central column (see Supplementary Material [22]). This helium environment is found to be similar to that of a helium-vacancy complex bound to the kink in its original position. Although this is technically the ground state for the helium-stabilised left kink, for it to exist in a kink pair the dislocation line would also have to be kinked in the [110] direction, which would be accompanied by a large energetic cost. Therefore, this rearrangement is not considered relevant within the scope of this letter.

Helium-assisted kink pair nucleation and hindered migration — The favourability of binding to the dislocation kinks leads to a proportionate decrease in the kink pair nucleation energy, providing the mechanism proceeds with helium bound to one of the kinks. Using the

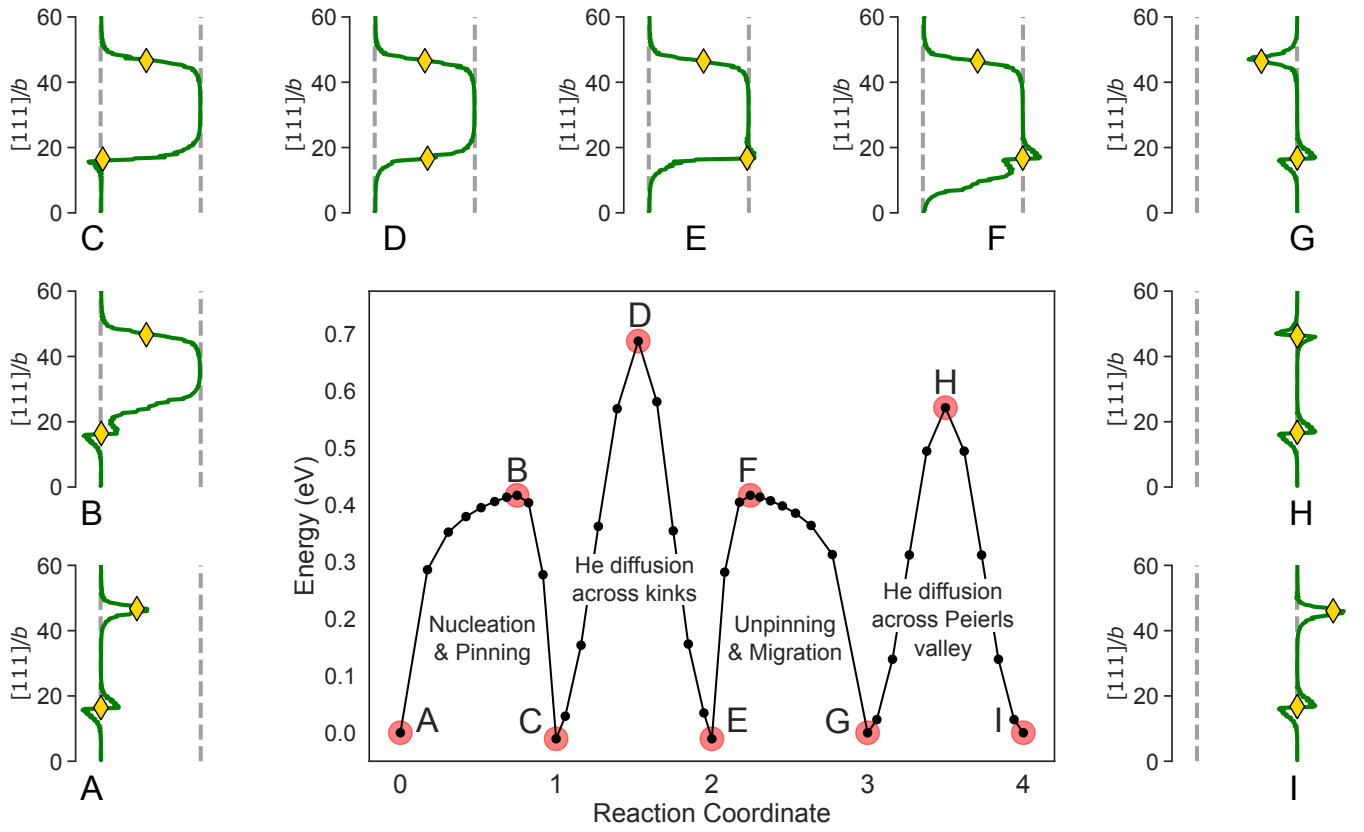


FIG. 4. Multi-step NEB pathway demonstrating helium-assisted kink pair nucleation and hindered kink migration. Dislocation line positions (determined using the cost function method [11]) as they move between Peierls valleys (grey dashed lines), for the key images are shown. Reaction coordinate is normalised by average dislocation position for A→C and E→G, and by helium position for C→E and G→I. Finite-size effects of similar size to Figure 3 exist for A→C and C→E, but are not quantified.

Nudged Elastic Band (NEB) method [23], we find that the most favourable mechanism involves helium stabilising the right kink, since $E_{RK,pref} > E_{LK,pref}$. For this to be observed, the helium must be situated next to the [111] atomic column that separates the initial Peierls valley from the next. The reconstruction to the split core local to the helium atom means that the dislocation line is already partially moved towards the next valley. As shown in Figure 3 (A→C), the kink pair nucleates at the helium, forming a helium-stabilised right kink and a left kink that is free to move laterally to propagate the dislocation to the next Peierls valley. The energy barrier from the NEB simulation is 0.43 eV; however, there is a 0.08 eV finite-size effect, giving the process a corrected barrier of 0.51 eV. This finite-size effect is quantified by comparing the kink pair nucleation energy obtained for pure tungsten in the same simulation setup (1.56 eV) with the converged value that is inexpensively obtained from the sum of the single kink energies ($E_{KP} = 1.64$ eV). There is a 14 meV perturbation ($E_{RK,diff}$) in the middle of the path that corresponds to helium crossing the central [111] column, since it does not sit exactly at the centre of the kink. To the best of our knowledge, this is the first report of significant impurity assistance to the kink pair

mechanism. A $\sim 10\%$ decrease in the nucleation energy has been observed in the Fe-H system, both with an embedded atom model [24] and a neural network potential [25]. The latter only partially demonstrated assistance, since the kink unpinned prematurely during the NEB simulation.

For this helium atom to repeatedly assist with dislocation motion, it must reposition itself adjacent to the next central [111] atomic column before each nucleation event (C→E, Figure 3). During this diffusion, the dislocation core local to the helium atom moves between split cores, whilst the dislocation as a whole remains in the same Peierls valley. Notably greater than the 63 meV barrier in bulk, we find that this process has a barrier of 0.57 eV (with negligible finite-size effects on diffusion events). The overall requirement for dislocation motion reduces from 1.64 eV in pure tungsten, to a pair of ~ 0.5 eV barriers in the presence of a single helium atom.

The mechanism that proceeds through the helium-stabilised left kink can also be probed, but the nucleation energy is only reduced to 1.21 eV, due to the lower preference for left kink binding. However, the diffusion barrier to advance the helium atom is less than 0.1 eV, since it is diffusing into the core, which is highly favourable. Nev-

ertheless, this is a not relevant pathway, due to the larger nucleation energy (NEB path shown in the Supplementary Material [26]).

At finite helium concentrations, there will be more than one helium atom bound to the dislocation. Therefore, kinks that are free to move may encounter helium atoms. The preference for kink binding — which assists nucleation — hinders kink migration since the kinks become pinned. For example, two isolated helium atoms on the dislocation line can advance the line by an entire Peierls valley through four events (Figure 4). (1) Nucleation through a helium-stabilised right kink and migration of the left kink until it is pinned by the second helium atom, forms a stable kink pair intermediate (A→C). Then, (2) diffusion of the helium across the left kink (0.68 eV) and (3) an unpinning event (to overcome $E_{\text{LK,pref}}$ and continue kink migration) are both required for the dislocation to advance, most favourably in that order (C→E and E→G). The two helium diffusion events from Figure 3 are also required, first at the right kink (incorporated into C→E for illustrative purposes, due to its negligible barrier) and finally (4) diffusion across the Peierls valley to the next [111] column (G→I). As the number of isolated helium atoms increases, the number of additional unpinning and diffusion events will also increase. Additionally, the evolution and influence of helium clusters will become relevant as the concentration increases. The stabilised kink pair (C, Figure 4) is similar in energy to the straight dislocation. Helium atom clustering at the kinks could lead to further stabilisation, creating a scenario where kinked dislocation lines are considerably more stable. This will be explored in future work, where we will explore whether a transition from softening to hardening occurs. This will require long timescale molecular dynamics to obtain meaningful statistics. The high stresses necessary to observe sufficient motion will increase the relevance of the unpinning of the helium from the dislocation line [27]. In order to investigate regimes of temperature and stress inaccessible by molecular dynamics, we plan to parameterise a kinetic Monte Carlo model to simulate dislocation velocity [28].

In summary, we have shown that the interaction of helium atoms with screw dislocations can have significant effects on their mobility, assisting kink pair nucleation and hindering kink migration. Extension of a previous tungsten MLIP for screw dislocations, to include disloca-

tion kinks and dilute helium-dislocation interactions, was required to access the necessary length and time scales. We note that the reported energy differences are sensitive to the details of the regression methodology, which would have exponential effects if propagated through rate laws. Although this study has focused on tungsten, we anticipate that similar phenomena would be observed for other impure body-centred cubic metals.

Atomic configurations, NEB image series and interactive visuals of dislocation core positions for the main results, as well as the *ab initio* database and resulting GAP model, are available from <https://zenodo.org/doi/10.5281/zenodo.11620483>.

Dislocation configurations were created and analysed mostly using tools available from the `matscipy.dislocation` module [29]. The atomic simulation environment was used to handle atomic configurations and run simulations [30], with an emphasis on `ase.calculators.lammpslib` (which depends on LAMMPS [31]), and the preconditioned minimisers in the `ase.optimize.precon` module [32, 33].

We thank James Turner and Shailesh Mehta for helpful discussions. MN is supported by a studentship funded by the UK Engineering and Physical Sciences Research Council-supported Centre for Doctoral Training in Modelling of Heterogeneous Systems, Grant No. EP/S022848/1 and the Atomic Weapons Establishment. JRK acknowledges funding from the Leverhulme Trust under grant RPG-2017-191. APB acknowledges support from the CASTEP-USER project, funded by the Engineering and Physical Sciences Research Council under the grant agreement EP/W030438/1. JRK and APB acknowledge funding from the NOMAD Centre of Excellence funded by the European Commission under grant agreement 951786. We acknowledge the University of Warwick Scientific Computing Research Technology Platform for assisting the research described within this study. Some of the calculations were performed using the Sulis Tier 2 HPC platform hosted by the Scientific Computing Research Technology Platform at the University of Warwick. Sulis is funded by EPSRC Grant EP/T022108/1 and the HPC Midlands+ consortium. We are grateful for computational support from the UK national high performance computing service, ARCHER2, for which access was obtained via the UKCP consortium and funded by EPSRC Grant No. EP/X035891/1.

[1] M. Rieth, S. L. Dudarev, S. M. Gonzalez de Vicente, J. Aktaa, T. Ahlgren, S. Antusch, D. E. J. Armstrong, M. Balden, N. Baluc, M.-F. Barthe, W. W. Basuki, M. Battabyal, C. S. Becquart, D. Blagoeva, H. Boldyryeva, J. Brinkmann, M. Celino, L. Ciupinski, J. B. Correia, A. De Backer, C. Domain, E. Gaganidze, C. García-Rosales, J. Gibson, M. R. Gilbert, S. Giusepponi, B. Gludovatz, H. Greuner, K. Heinola, T. Höschel, A. Hoffmann, N. Holstein, F. Koch, W. Krauss, H. Li,

S. Lindig, J. Linke, C. Linsmeier, P. López-Ruiz, H. Maier, J. Matejcek, T. P. Mishra, M. Muhammed, A. Muñoz, M. Muzyk, K. Nordlund, D. Nguyen-Manh, J. Opschoor, N. Ordás, T. Palacios, G. Pintsuk, R. Pippan, J. Reiser, J. Riesch, S. G. Roberts, L. Romaner, M. Rosiński, M. Sanchez, W. Schulmeyer, H. Traxler, A. Ureña, J. G. van der Laan, L. Veleva, S. Wahlberg, M. Walter, T. Weber, T. Weitkamp, S. Wurster, M. A. Yar, J. H. You, and A. Zivelonghi, *J. Nucl. Mater.* **432**,

- 482 (2013).
- [2] M. R. Gilbert, S. L. Dudarev, S. Zheng, L. W. Packer, and J.-C. Sublet, *Nucl. Fusion* **52**, 083019 (2012).
- [3] A. Hasegawa, Y. Sato, T. Hattori, R. Kanamaru, L. Du, T. Miyazawa, and S. Nogami, *Nucl. Eng. Des./Fusion* **29**, 101076 (2021).
- [4] P. Grigorev, A. M. Goryaeva, M.-C. Marinica, J. R. Kermode, and T. D. Swinburne, *Acta Mater.* **247**, 118734 (2023).
- [5] T. D. Swinburne and J. R. Kermode, *Phys. Rev. B Condens. Matter* **96**, 144102 (2017).
- [6] S. Klawohn, J. R. Kermode, and A. P. Bartók, *Mach. Learn.: Sci. Technol.* **4**, 015020 (2023).
- [7] S. Klawohn, J. P. Darby, J. R. Kermode, G. Csányi, M. A. Caro, and A. P. Bartók, *J. Chem. Phys.* **159** (2023).
- [8] W. J. Szlachta, A. P. Bartók, and G. Csányi, *Phys. Rev. B Condens. Matter Mater. Phys.* **90** (2014).
- [9] S. J. Clark, M. D. Segall, C. J. Pickard, P. J. Hasnip, M. I. J. Probert, K. Refson, and M. C. Payne, *Zeitschrift für Kristallographie - Crystalline Materials* **220**, 567 (2005).
- [10] L. Ventelon and F. Willaime, *Journal of Computer-Aided Materials Design* **14**, 85 (2007).
- [11] L. Ventelon, F. Willaime, E. Clouet, and D. Rodney, *Acta Mater.* **61**, 3973 (2013).
- [12] E. Clouet, L. Ventelon, and F. Willaime, *Phys. Rev. Lett.* **102**, 055502 (2009).
- [13] (2024), see supplemental material at <https://zenodo.org/doi/10.5281/zenodo.11620483> for more information about our MLIP database, fitting and use.
- [14] J. P. Perdew, K. Burke, and M. Ernzerhof, *Phys. Rev. Lett.* **77**, 3865 (1996).
- [15] J. Byggmästar, A. Hamedani, K. Nordlund, and F. Djurabekova, *Phys. Rev. B Condens. Matter* **100**, 144105 (2019).
- [16] C. S. Becquart and C. Domain, *Phys. Rev. Lett.* **97**, 196402 (2006).
- [17] (2024), see supplemental material at <https://zenodo.org/doi/10.5281/zenodo.11620483> for helium-induced core reconstruction in saturated regime visuals.
- [18] A. Stukowski, *Modell. Simul. Mater. Sci. Eng.* **18**, 015012 (2009).
- [19] L. Ventelon, F. Willaime, and P. Leyronnas, *J. Nucl. Mater.* **386-388**, 26 (2009).
- [20] S. Chiesa, P. M. Derlet, S. L. Dudarev, and H. Van Swygenhoven, *J. Phys. Condens. Matter* **23**, 206001 (2011).
- [21] V. V. Bulatov, J. F. Justo, W. Cai, and S. Yip, *Phys. Rev. Lett.* **79**, 5042 (1997).
- [22] (2024), see supplemental material at <https://zenodo.org/doi/10.5281/zenodo.11620483> for left kink reconstruction visuals.
- [23] G. Henkelman, B. Uberuaga, and H. Jónsson, *J. Chem. Phys.* **113**, 9901 (2000).
- [24] L. Huang, D. Chen, D. Xie, S. Li, Y. Zhang, T. Zhu, D. Raabe, E. Ma, J. Li, and Z. Shan, *Nat. Mater.* **22**, 710 (2023).
- [25] F.-S. Meng, J.-P. Du, S. Shinzato, H. Mori, P. Yu, K. Matsubara, N. Ishikawa, and S. Ogata, *Phys. Rev. Mater.* **5**, 113606 (2021).
- [26] (2024), see supplemental material at <https://zenodo.org/doi/10.5281/zenodo.11620483> for left kink stabilised nucleation NEB pathway.
- [27] A. Allera, F. Ribeiro, M. Perez, and D. Rodney, *Phys. Rev. Mater.* **6**, 013608 (2022).
- [28] A. Stukowski, D. Cereceda, T. D. Swinburne, and J. Marian, *Int. J. Plast.* **65**, 108 (2015).
- [29] P. Grigorev, L. Frérot, F. Birks, A. Gola, J. Golebiowski, J. Griebner, J. L. Hörmann, A. Klemenž, G. Moras, and W. G. Nöhring, *Journal of Open Source Software* **9** (2024).
- [30] A. Hjorth Larsen, J. Jørgen Mortensen, J. Blomqvist, I. E. Castelli, R. Christensen, M. Dułak, J. Friis, M. N. Groves, B. Hammer, C. Hargus, E. D. Hermes, P. C. Jennings, P. Bjerre Jensen, J. Kermode, J. R. Kitchin, E. Leonhard Kolsbjerg, J. Kubal, K. Kaasbjerg, S. Lysgaard, J. Bergmann Maronsson, T. Maxson, T. Olsen, L. Pastewka, A. Peterson, C. Rostgaard, J. Schiøtz, O. Schütt, M. Strange, K. S. Thygesen, T. Vegge, L. Vilhelmsen, M. Walter, Z. Zeng, and K. W. Jacobsen, *J. Phys. Condens. Matter* **29**, 273002 (2017).
- [31] A. P. Thompson, H. M. Aktulga, R. Berger, D. S. Bolintineanu, W. M. Brown, P. S. Crozier, P. J. in 't Veld, A. Kohlmeyer, S. G. Moore, T. D. Nguyen, R. Shan, M. J. Stevens, J. Tranchida, C. Trott, and S. J. Plimpton, *Comput. Phys. Commun.* **271**, 108171 (2022).
- [32] D. Packwood, J. Kermode, L. Mones, N. Bernstein, J. Woolley, N. Gould, C. Ortner, and G. Csányi, *J. Chem. Phys.* **144**, 164109 (2016).
- [33] S. Makri, C. Ortner, and J. R. Kermode, *J. Chem. Phys.* **150**, 094109 (2019).